World Academy of Science, Engineering and Technology
International Journal of Mechanical and Mechatronics Engineering
Vol:8, No:12, 2014

Calibration of the Discrete Element Method Using a Large Shear Box

Corné J. Coetzee, Etienne Horn

***Abstract*—**One of the main challenges in using the Discrete Element Method (DEM) is to specify the correct input parameter values. In general, the models are sensitive to the input parameter values and accurate results can only be achieved if the correct values are specified. For the linear contact model, micro-parameters such as the particle density, stiffness, coefficient of friction, as well as the particle size and shape distributions are required. There is a need for a procedure to accurately calibrate these parameters before any attempt can be made to accurately model a complete bulk materials handling system. Since DEM is often used to model applications in the mining and quarrying industries, a calibration procedure was developed for materials that consist of relatively large (up to 40 mm in size) particles. A coarse crushed aggregate was used as the test material. Using a specially designed large shear box with a diameter of 590 mm, the confined Young's modulus (bulk stiffness) and internal friction angle of the material were measured by means of the confined compression test and the direct shear test respectively. DEM models of the experimental setup were developed and the input parameter values were varied iteratively until a close correlation between the experimental and numerical results was achieved. The calibration process was validated by modelling the pull-out of an anchor from a bed of material. The model results compared well with experimental measurement.

***Keywords*—**Discrete Element Method (DEM), calibration, shear box, anchor pull-out.

I. Introduction

THE use of the Discrete Element Method (DEM) in the numerical modelling of bulk material handling processes and systems has become very popular in recent years. Advances in computing resources have resulted in the increased usage of DEM as a design validation and optimization tool as opposed to expensive physical prototyping [1]-[3]. It is estimated that 40% of the capacity of industrial plants are wasted because of bulk handling problems [4]. Considering the scale and importance of bulk material handling operations in industry, ranging from the mining and pharmaceutical to the agricultural industries, the positive economic impact of more efficient systems, from a design and operational point of view, cannot be ignored.

A crucial element of discrete element modelling lies in the acquisition of an accurate set of material input parameter values. Since natural bulk materials are affected by external conditions and geographic location, obtaining the appropriate input parameter values can become very challenging. In some cases the calibration of the bulk material can be the largest component of a DEM simulation project. Therefore a clear need exists for calibration procedures that are more efficient from both an experimental and numerical point of view. Robust experimental tests are required that can quantify most of the desired bulk material properties and also provide for the effective comparison to the DEM input parameters.

We distinguish between the material macro-properties and the DEM micro-parameters. Material macro-properties are bulk properties that can be measured in the field or using laboratory equipment. This for example includes resistance to penetration, the angle of repose, the bulk density, the internal friction angle (shear test) and the bulk stiffness (compression test). The micro-parameters on the other hand, are the parameters used by the specific discrete element method to model the material. This for example includes the particle stiffness, the particle-particle friction coefficient and the particle density. It is much more difficult to accurately measure the micro-parameter values experimentally and even if this can be done, it does not necessarily mean that the DEM model would show the same level of accuracy on a bulk level. This approach would only be accurate if the shape of the particles is modelled accurately and if the modelled particles have the same size as the real particles. This is very difficult to achieve when industrial scale systems are modelled where the particle size has to be increased [5] and the particle shape cannot be accurately modelled. It is very difficult to accurately model the shape of most real particles unless the particles happen to be spheres [6], [7] or specific shapes tested in laboratories. For this reason very few researchers have tried to measure the micro-parameters experimentally. Reference [8] measured the coefficient of restitution in soybeans using drop tests. Reference [9] measured the micro-parameters of maize grains and olives and validation was performed by modelling silo discharge [10].

Our approach is to perform laboratory experiments where the macro-properties can be measured and then through a reverse calibration process, the experiments are repeated numerically and an iterative process is used to find the micro-parameter values. A similar process was used by [11]-[13] where corn grains were used as material. In this study, however, we focus on gravel with particles up to 40 mm in size [14].

Several authors made use of a similar strategy. Reference [15] modelled soil-tool interaction and made use of an iterative process to obtain the DEM parameter values. However, they did not propose a general calibration

C. J. Coetzee is with the Department of Mechanical & Mechatronic Engineering, Stellenbosch University, Stellenbosch, South Africa (phone: +27 (0)21 808 4239 fax: +27 (0)21 808 4958 ; e-mail: ccoetzee@sun.ac.za).

E. Horn was a Master student with the Department of Mechanical & Mechatronic Engineering, Stellenbosch University, Stellenbosch, South Africa.

procedure, but rather used the draft force on a blade to set the parameter values. Reference [5] made use of direct shear tests and a newly developed slump-tester to determine the input parameter values of polyethylene pellets.

Reference [16] conducted bar penetration tests and compared the results with those obtained from DEM simulations. The contact stiffness was chosen without any experimental validation and by comparing the movement of the particles during the experiment with the movement of the particles during the simulation, the friction coefficient could be determined. Reference [17] proposed an inverse calibration method to determine the micro-parameter values. Based on DEM results, the particle friction coefficient and stiffness were determined from energy principles and direct shear tests. References [18], [19] proposed an in-situ method for determining the micro-parameter values. Their method was based on wedge penetration tests and a non-linear optimization scheme. The methodology was validated by using DEM simulation results instead of real in-situ tests.

The main objective of this study was to perform a calibration process on a natural material with relatively large particles to demonstrate the applicability to mining bulk materials handling processes. For this purpose, a large shear box that could accommodate a coarse aggregate (up to 40 mm in size) was designed and built. To validate the calibration process, the calibrated parameter values were used to model anchor pull-out and the pull-out forces were compared to experimental measurements. The commercial DEM software package, PFC^{3D}, was used in this study [20].

II. The Discrete Element Method

Discrete element methods are based on the simulation of the motion of granular material as separate particles [21]. Using the soft particle approach, each contact is modelled with a linear spring in the contact normal direction (secant stiffness k_{cn}) and a linear spring in the contact tangential direction (tangent stiffness k_{cs}) as depicted in Fig. 1. Frictional slip is allowed in the tangential direction with a friction coefficient μ. The particles are allowed to overlap and the amount of overlap is used in combination with the spring stiffness to calculate the contact force components. The contact force in the normal direction is given by [20],

$$F_n = k_{cn} U_n \tag{1}$$

where U_n is the overlap in the contact normal direction. The contact shear force is given by

$$F_s = \begin{cases} \sum k_{cs} \Delta U_s & \text{for } |F_s| < |\mu F_n| \\ \mu F_n \text{sign}\left(\sum \Delta U_s\right) & \text{for } |F_s| \geq |\mu F_n| \end{cases} \tag{2}$$

where ΔU_s is the displacement increment in the contact tangential direction. This is the basic linear contact model as found in most DEM codes and used in this study. Non-linear models such as the Hertz model [20] and the Walton-Braun model [22] are also available, but are usually computationally less efficient [23]. In general, cohesion can be modelled using bonds at the contacts [24], [20]. In this study only cohesionless material was considered and bonds were not needed.

Besides contact friction, PFC^{3D} has two other standard mechanisms for the dissipation of energy. Damping can be applied at the contacts through a viscous dashpot in the normal and the tangential direction, or at local level. When local damping is applied, a damping-force term is added to the equations of motion [20],

$$\overline{F}_d = -\alpha \left|\overline{F}_R\right| sign\left(\overline{V}\right) \tag{3}$$

where $\overline{F}_d$ is the damping force vector applied to the particle, $\overline{F}_R$ is the resultant force acting on the particle (due to contact with other particles or walls and gravity), $\overline{V}$ is the particle velocity vector and α is the damping constant. For a detailed description of DEM, the reader is referred to [20], [21], [25]-[27].

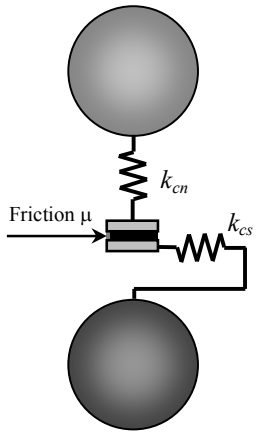

Fig. 1 Linear contact model used in DEM

III. The Large Shear Box

The direct translational shear test (Jenike shear cell) is commonly used to determine the bulk properties of granular materials [28]. The shear box is typically constructed of two halves, namely a top and a bottom half. The sample is sheared laterally by moving either the top or bottom half relative to the other, while simultaneously applying a normal load on the sample. This shear displacement normally occurs at a constant velocity. It is mostly assumed that this action induces a thin, well defined shear zone for finer grained materials [29]. The mean normal and shear stress acting on this horizontal plane are calculated from the measured normal and shear loads and subsequently used to determine bulk properties such as the internal friction angle [29].

Reference [30] suggested a bin diameter to particle size ratio of more than 8 for a similar test setup. The confined compression test was also performed using the large scale shear box's container and for this test, [30] suggested a sample

height to particle size ratio of approximately 10. The design was therefore done according to these guidelines.

The shear box consisted of a cylindrical container, divided into a top and a bottom half. The container had an inner diameter of 590 mm and a total height of 330 mm. The top half of the container was fixed to a support frame, while the bottom half rested on a set of tracks, thus enabling it to be moved horizontally on steel castor wheels. The tracks also formed part of the frame, Fig. 2.

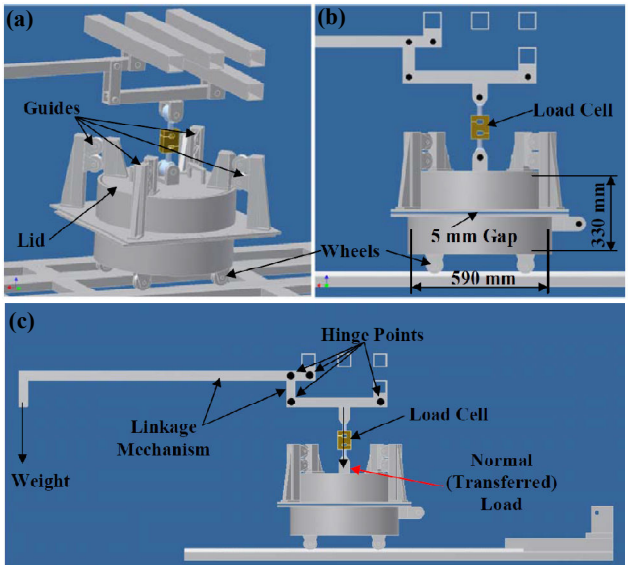

Fig. 2 The large shear box showing (a) the lid with guides and the bottom half on castor wheels, (b) the dimensions and position of the normal load cell and (c) the linkage mechanism to apply the normal load. The hydraulic actuator was attached between the bottom half and the frame

The bottom half was connected to a hydraulic actuator, which was mounted on the support frame. To facilitate the normal load on the sample, a lid was placed on top of the sample. Three guides were used to prevent the lid from twisting and to keep it as level as possible during the tests. The normal load was applied by means of a linkage mechanism that was connected to the lid. A gap of roughly 5 mm existed between the top and bottom half as to induce a shear effect in the bulk material sample only, eliminating any steel-on-steel friction between the top and bottom halves. The linkage was designed so that the normal load that the lid experienced was approximately 42 times the load attached to the end of the linkage. It should be noted that the weight of the linkage itself, as well as that of the lid, also contributed to the normal load on the sample.

The horizontal displacement of the bottom half of the container was provided by the hydraulic actuator. To provide the constant shear velocity needed for the shear test, the motion of the cylinder was controlled by means of a PID controller and a PLC interface. Through this control, a constant shear velocity of 1 mm·s^{-1} could be applied over a total shear distance of 70 mm.

Two commercially available 50 KN load cells (HBM S9) were used to measure the normal load on the lid and the shear force on the bottom half respectively. The vertical displacement of the lid, as well as the horizontal displacement of the bottom half, was recorded with an HBM WA L linear variable differential transducer (LVDT). All four of these sensors were connected to an HBM Spider8 data logger and the data acquisition was performed by means of HBM Catman software at a sampling frequency of 50 Hz. The friction force experienced by the moving bottom half was measured under varying normal loads and subtracted from the measured shear forces during the tests.

IV. Calibration of Material Parameters

With only cohesionless material under consideration, the DEM parameters under investigation were the particles size and shape, particle density, particle-particle friction coefficient, particle contact stiffness, particle-wall friction coefficient, wall contact stiffness and the contact damping.

Note that, in PFC^{3D} the normal and shear stiffness of the particles (k_{pn} and k_{ps}) and the normal and shear stiffness of the walls (k_{wn} and k_{ws}) are specified and are not the contact stiffness (k_{cn} and k_{cs}) as shown in Fig. 1. At run time, the contact stiffness is calculated at each contact, using two linear springs in series. These two springs are either particle-particle springs or particle-wall springs depending on the specific contact. It was also assumed that the particle shear stiffness, k_{ps}, has the same value as the particle normal stiffness, k_{pn}. From here onwards the particle stiffness is denoted by $k_p = k_{ps} = k_{pn}$. The same applies to the wall stiffness denoted by $k_w = k_{ws} = k_{wn}$ and hence the contact stiffness given by $k_c = k_{cs} = k_{cn}$. Several authors also set the shear stiffness equal to the normal stiffness [15], [19], [31].

A. Damping and Wall Stiffness

The damping was very difficult to measure. Due to the irregular particle shapes, drop tests would not provide consistent results. It was assumed that the material had a fairly high damping coefficient and that all the calibration tests were quasi-static in nature. Therefore a contact critical damping ratio of 0.8 was used in all the models [20].

The wall stiffness, k_w, was set to a value roughly one order higher than the particle stiffness to ensure rigid walls. When a particle comes into contact with a wall, the particle stiffness and the wall stiffness act like two springs in series, resulting in a contact stiffness given by,

$$k_c = \frac{k_p k_w}{k_p + k_w} \tag{4}$$

with a zero wall stiffness and a given particle stiffness, the contact stiffness is zero. As the wall stiffness is increased, the contact stiffness increases non-linearly and approaches an asymptotic value equal to k_p. In general, the contact stiffness cannot be higher than the lower of the two stiffness in series. In this study, a wall stiffness of $k_w = 10 \cdot 10^6$ N·m^{-1} was used in all the models. Using the calibrated particle stiffness, this resulted in a contact stiffness which was roughly 90% of the

asymptotic value.

B. Particle-Wall Friction Coefficient

A basic experimental procedure was used to estimate the particle-wall friction coefficient, μ_w, for each of the interface (wall) materials in this study. The experiment consisted of a rock particle that was placed on a flat surface of the interface material. The surface was then carefully tilted while the inclination angle was recorded with a digital protractor. The angle at which the particle started to slide down the surface was noted. The sliding angle, γ, was then used to calculate the particle-wall friction coefficient, $\mu_w = \tan\gamma$. A similar approach was followed by [32]. Each test was repeated 25 times and the average friction coefficient with bare mild steel (anchor pull-out test) was found to be $\mu_w = 0.54$ and with coated mild steel (shear box) it was $\mu_w = 0.62$. These values were directly implemented in the DEM model.

C. Particle Size and Shape

Crushed rock from a roller mill with a 25 mm clearance between the rollers was used as material. A random sample of roughly 300 rocks was taken and the rocks could be classified into three distinct particle shapes. These shapes were kept as simple as possible, while ensuring that every rock in the sample belonged to one of the particle shapes. The particle shapes were (Fig. 3): a so-called pyramid shape, an elongated shape and a largely spherical shape. The rock sample was classified according to the above shapes and the number of particles belonging to each shape was recorded and a particle shape distribution was obtained. It was found that the spherical particles comprised approximately 21% of the total sample, while the pyramid shape comprised 37% and the elongated shape 42%. This data was then used to ensure that the same distribution between particle shapes was maintained when generating particles for the DEM model.

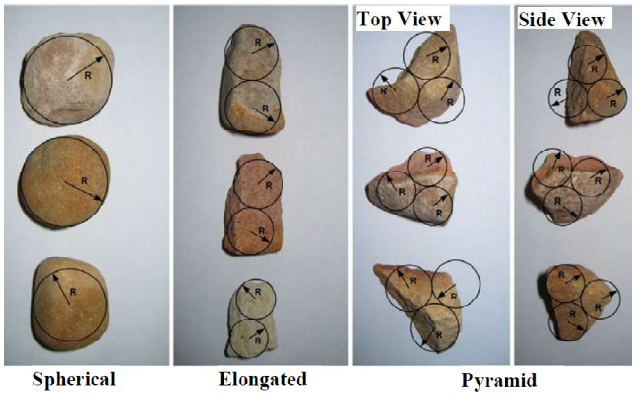

Fig. 3 The identified particle shapes with the clump equivalents superimposed

In a DEM model, when using spherical particles, the bulk friction of the material (assembly of particles) is usually too low when compared to real granular material like crushed rock. Non-spherical particles are needed to increase the particle interlocking effect and one solution is to make use of clumped particles [33], [34]. Clumps can be formed by adding two or more spherical particles together to form one rigid particle, i.e. particles comprising the clump remain at a fixed distance from each other [20]. Particles within a clump can overlap to any extent and contact forces are not generated between these particles. Clumps cannot break up during simulations regardless of the forces acting in on them.

When laboratory setups are modelled in DEM, it might be possible to accurately model the size of the particles. However, when large scale industrial applications are modelled, it would normally not be possible to accurately model the particle size since it would be computationally too demanding. In order to decrease the total number of particles, it is possible to increase the particle size. It has been shown by [35] and [36] that particles can be scaled up in size and still the draft force in soil can be accurately predicted.

In this study, however, the actual size of the particles was modelled accurately. The clump representations of the particle shapes can be seen in Figs. 3 and 4. The elongated particles were represented by two spheres clumped together, while the pyramid shaped particles were represented by four spheres clumped together as shown in Fig. 4. Where the particle shape was largely spherical, representation by means of a single sphere was deemed appropriate. A Gaussian distribution was used to generate the clumps in PFC^{3D} with the minimum and maximum radii 15.0 mm and 16.2 mm for the spherical particles, 12.0 mm and 15.0 mm for the elongated particles and 7.5 mm and 10.5 mm for the pyramid shaped particles respectively. The factor C in Fig. 4 ranges from zero to one and is used to set the centre distance between the balls in the clump. The centre distance is given by $2CR$ where R is the ball radius. In this study, $C = 1$ was used.

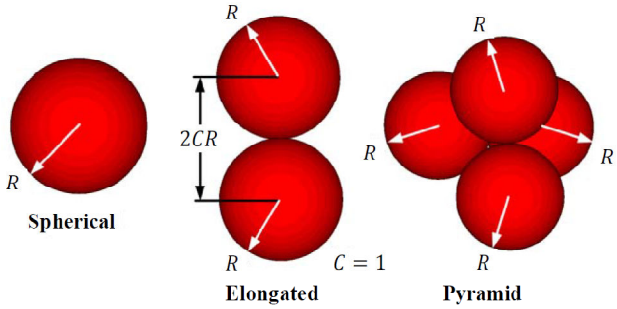

Fig. 4 Clump particle representation

D. Particle Density, Bulk Density and Porosity

The bulk density is defined as the mass of a bulk material sample divided by the bulk volume (including the voids between the particles) that the sample occupies [37]. The bulk density was easily determined by filling a container of a known volume with a sample from the bulk material. The bulk mass, m, of the material that was placed in the container was recorded and used, along with the container volume, V_b, to calculate the bulk density, $\rho_b = m / V_b$. For this purpose, the shear box was used as the container, and the results from three samples were 1412.0 kg·m^{-3}, 1383.6 kg·m^{-3} and 1397.8 kg·m^{-3} respectively with an average value of ρ_b =1397.8 kg·m^{-3}.

The particle density was determined by weighing a small

sample of particles (between 0.5 kg and 1 kg) and determining the volume of that same sample by submerging it under water and measuring the volume of the displaced water. It was assumed that the particles did not absorb any water during the short time the experiment was conducted. This procedure was repeated for ten samples, resulting in an average particle density $\rho_p = 2586.5$ kg·m^{-3}.

The porosity is defined as the ratio between the void volume, V_v, and the bulk (total) volume [37], $n = V_v / V_b = 1 - \rho_b / \rho_p$. The measured results from the three samples were 0.45, 0.47 and 0.46 with an average value of $n = 0.46$.

In the DEM model the aim would be to accurately model the bulk density since the final goal is to accurately model the bulk behaviour of an anchor pull-out test. This was achieved by filling a DEM model of the shear box with the clumped particles. At this stage of the calibration process, the particle stiffness and particle friction were still unknown. However, the bulk density was not strongly dependent on either of these two parameters (within a realistic range) and the process followed here was an iterative process, so that the density calibration was revisited. In the first iteration, a particle stiffness was set to $k_p = 1{\cdot}10^6$ N·m^{-1} and the particle friction to $\mu_p = 0.1$. The particle-wall friction coefficient was set to $\mu_w = 0.62$ as measured. With all the other parameters fixed, the bulk density varied linearly with a change in the particle density. An iterative process was used to determine the particle density as $\rho_p = 2500$ kg·m^{-3} which resulted in a bulk density of $\rho_b = 1398.0$ kg·m^{-3} (close to the measured bulk density).

The particle density was slightly different from the measured value, $\rho_p = 2586.5$ kg·m^{-3}. The aim was to model the bulk density accurately, and not necessarily the particle density. However, if the particle size and shape was more accurately modelled, then the resulting particle density in the DEM model would also be very close to the actual particle density. In this case we managed to achieve this with an error of 3.3%. This means that the modelled porosity, $n = 0.44$, was also close to the measured value, $n = 0.46$. If it was necessary to model the porosity more accurately, the modelling of the particle shape and size would have to be revisited. An example of where the porosity plays an important role is the modelling of thermal rock beds where the rocks are modelled by DEM, followed by CFD modelling of air flow through the bed [38].

E. Confined Compression Tests

Confined uniaxial stress loading is often used in geotechnical engineering to measure soil consolidation, called the oedometer test [39]. The normal load is increased to a certain maximum load, after which it is reduced again to a zero load. This loading and unloading process constitutes one compression cycle, which is repeated a number of times to complete the test. The normal load and resulting normal displacement are recorded and the bulk longitudinal stress and strain calculated.

In this study the shear box was used, but instead of applying a shearing load, the lid of the shear box was used to apply a compression load. The shear box was filled with material, the bed carefully levelled and the initial height measured. The lid was then placed on top of the bed and the load on the linkage was increased in increments of 10 kg until a maximum of 40 kg was reached, resulting in a maximum normal stress on the bed of approximately 65.6 kPa. The load was then decreased in increments of 10 kg until only the linkage and lid was left. Three of these loading-unloading cycles were completed per test, and three tests were conducted to ensure repeatability.

A typical stress-strain curve is shown in Fig. 5. During the first cycle, as expected, the packing settled and collapsed under the normal load due to inter-particle movements. For the second and third cycles the normal stress showed an almost linear relation to the normal strain. The confined Young's Modulus was obtained by calculating the average of the gradients for the second and third loading cycles. The whole test was repeated three times and the average confined Young's Modulus was obtained as 8.96 MPa.

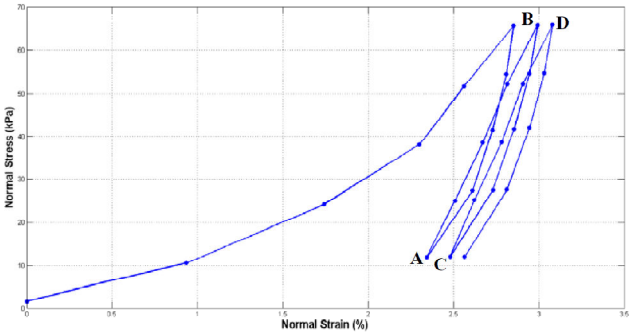

Fig. 5 A typical result from a compression experiment. The second loading is from point A to point B and the third loading from point C to point D

The next step was to perform the confined compression test numerically. The exact dimensions of the container (shear box) used in the experiment were used to build a DEM model of the confined compression test and the container was filled with the clumped particles. At this stage in the calibration process, only the particle friction and particle stiffness had not yet been calibrated. References [11] and [12] have shown that the confined compression test is not sensitive to the particle friction and that there is a linear relation between the confined Young's modulus and the particle stiffness. Therefore, the particle friction was kept at μp = 0.1 and the confined compression test was modelled using particle stiffness values of $1.0{\cdot}10^6$ N·m^{-1}, $1.7{\cdot}10^6$ N·m^{-1}, $2.3{\cdot}10^6$ N·m^{-1} and $3.0{\cdot}10^6$ N·m^{-1}. The calibrated particle density of 2500 kg·m^{-3} was used, along with a particle-wall friction coefficient of $\mu_w = 0.62$. Fig. 6 shows a typical stress-strain curve from the DEM model. The same procedure as used in the experiments was used to determine the confined Young's modulus for each particle stiffness value used. These results are given in Fig. 7. Using a linear fit and the measured confined Young's modulus of 8.69 MPa, the particle stiffness was interpolated and a value of $k_p = 1.72{\cdot}10^6$ N·m^{-1} was obtained. This new particle stiffness of $1.72{\cdot}10^6$ N·m^{-1} was then used in another confined compression simulation without changing any of the other

parameters. It resulted in a confined Young's Modulus of 9.15 MPa and a simulated bulk density of ρ_b = 1397.1 kg·m^{-3}.

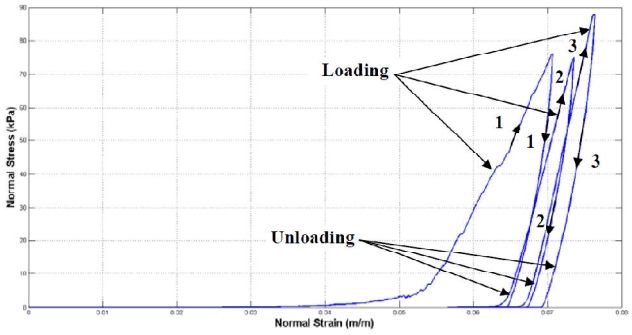

Fig. 6 A typical result from a compression simulation showing the loading and unloading cycles

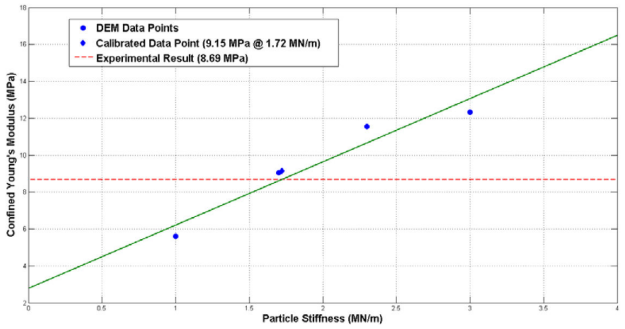

Fig. 7 The confined Young's modulus as a function of the particle stiffness

It should be noted that under some conditions it is possible to reduce the particle stiffness without significantly influencing the results. The critical time step size is inversely proportional to the square root of the stiffness and by reducing the stiffness, computational time can be reduced. It was shown by [40] that by reducing the stiffness by a factor 100 from the measured value had no significant influence on the rod penetration force into a granular material. Also, [41] showed that by reducing the stiffness by a factor 1000 had no significant influence on the material discharge rate or flow patterns from a silo. They conclude that the particle stiffness do not have a significant influence on the material behaviour under gravity driven flow. On the other hand, [15] showed that the draft force on a tool increased with an increase in the particle stiffness. A detailed study was done by [42] on the effects of reduced particle stiffness on the bulk response. They showed that the particle stiffness had a significant effect on the bulk stiffness and bulk restitution coefficient, it also had an effect on the angle of repose and the penetration force of a wedged shape tool. They conclude that the average particle overlap should be less than 0.3% of the particle radius and that users should be cautious to simply reduce the particle stiffness. In this study, reduction of the particle stiffness to reduce computational time was not implemented or investigated.

F. Direct Shear Tests

The next and last step in the calibration process was to determine the particle-particle friction coefficient, μp. For this purpose, the direct shear test was used. Fig. 8 shows a typical shear stress-strain curve from the experiment using normal loads of 10.5 kPa, 24.0 kPa, 38.3 kPa and 52.4 kPa. Here it is important to note that in general, the material properties are stress dependent [43]. Therefore, the normal stresses used should be in the range that the material will experience in the application that will finally be modelled. In this case the anchor pull-out test was used for validation and the parameters had to be calibrated for this application. It was estimated that the material in the anchor test would experience stresses in the order of 20 kPa.

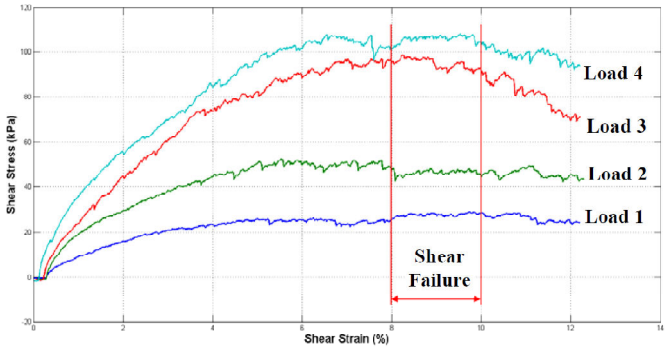

Fig. 8 A typical stress-strain curve from a shear experiment showing the shear load for four different normal loads

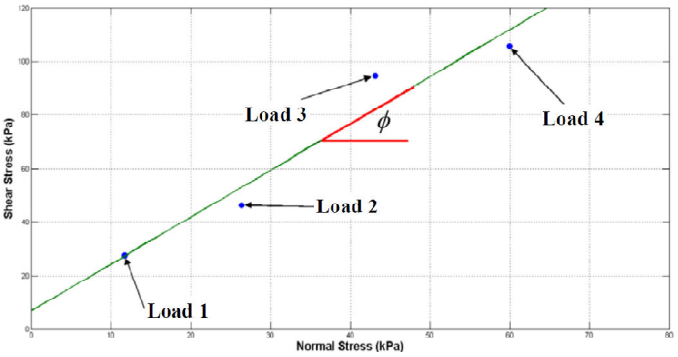

Fig. 9 The maximum shear stress from four normal loads plotted against the normal stress to define the friction angle φ

Fig. 9 shows the maximum shear stress plotted against the normal stress. Two values of the shear stress were used, the maximum value and the residual value. The maximum shear stress was simply taken as the maximum measured stress, while the residual stress was taken as the average of the shear stress between 8% and 10% shear strain. A linear relation was assumed and the slope of the line gave the internal friction angle. Three tests were conducted, and for each test the maximum and residual values were calculated. Taking the maximum and the minimum of all measurements (using maximum and residual stress), the internal friction angle varied between φ = 50.1° and φ = 56.3° with an average of

$\varphi = 52.8°$.

It was shown by [11], [42] that the shear test results (internal friction angle) from DEM simulations are highly influenced by both the particle friction and the particle stiffness (for low stiffness values). Therefore it is important to first calibrate the particle stiffness before the shear test is modelled. Using the calibrated parameters and particle friction coefficients of μ_p = 0.1, 0.3, 0.5, 0.7, 0.9 and 1.1 the shear tests were repeated numerically. The same four normal loads used in the experiments were applied and this resulted in stress-strain curves similar to those in Fig. 8. In each case the maximum shear stress and the residual shear stress (defined between 8% and 10% strain) were calculated. The average internal friction angle for each test is plotted in Fig. 10. It is clear that the relation between the values for particle friction coefficient and the material internal friction angle is not linear, and that it approaches an asymptotic value. Comparing the results with the experimental results, a final value of $\mu_p = 0.86$ was used for the particle friction coefficient.

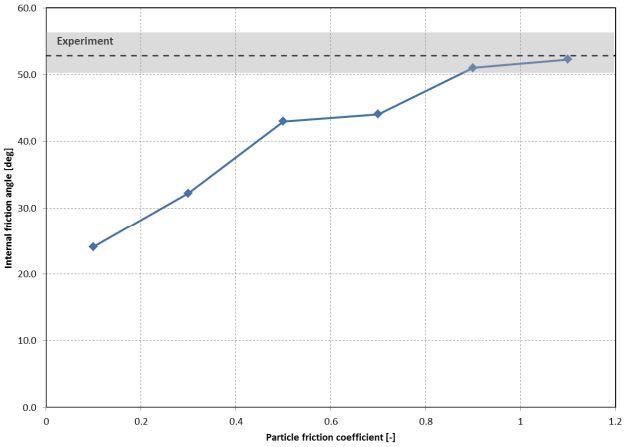

Fig. 10 The internal friction angle as a function of the particle friction coefficient. The experimental results fell in the shaded band shown with the average indicated by the dotted line

G. Iterative Process

The calibration process used here was an iterative process since the parameter values were determined one at a time and an educated guess was used to set the yet unknown parameter values. However, the order of calibration was chosen in such a way that the yet unknown parameter values had little effect on the calibration method used to determine the parameter value under consideration [11]. The micro-parameter values obtained after the first iteration were used in the second iteration and the calibration process repeated starting from the density. In this case, none of the micro-parameter values had to be adjusted, even though some of the macro-properties changed slightly but were still deemed accurate enough. The final set of micro-parameter values and macro-properties are summarized in Table I. In other cases, and if the initial estimate of the unknown parameter values used during the first iteration is not accurate enough, a second or even third iteration might be needed to obtain the final set of calibrated parameter values.

TABLE I
MATERIAL MICRO- AND MICRO PARAMETER VALUES

Symbol	Quantity	DEM	Experiment
ξ	viscous damping ratio	0.8	-
μ_w	particle-wall friction coefficient [a]	0.54; 0.62	0.54; 0.62
k_w	wall stiffness	$10 \cdot 10^6$ N·m^{-1}	-
ρ_p	particle density	2500 kg·m^{-3}	2586.5 kg·m^{-3}
k_p	particle stiffness	$1.72 \cdot 10^6$ N·m^{-1}	-
μ_p	particle-particle friction coefficient	0.86	-
ρ_b	bulk density	1395.8 kg·m^{-3}	1397.8 kg·m^{-3}
n	porosity	0.44	0.46
E'	Confined Young's modulus	6.95MPa	8.62 MPa
φ	internal friction angle	51.0°	52.8°

[a] Values for uncoated and coated mild steel respectively

V. ANCHOR PULL-OUT TESTS

An anchor pull-out test was used to validate the calibrated parameter values. The test entailed embedding, or anchoring a structure in a bed of bulk material and then slowly pulling it out of the bed while measuring the resistance force of the material on the anchor as it was pulled out.

A. Experimental Setup

The experimental set-up with dimensions is shown in Fig. 11. The system consisted of a bin, in which an anchor was placed vertically. The anchor was constructed from square tubing (50 mm x 50 mm x 3 mm), cut to a length of 1 000 mm, with a 110 mm x 110 mm x 5 mm mild steel plate welded to the one end. A load cell (HBN S9 50 kN) was connected to the anchor, after which the anchor was pulled out of the packing at a constant vertical speed. Different combinations of pull-out speeds and initial anchor depths were tested. The speeds tested were 27 mm·s^{-1} and 153 mm·s^{-1} and the initial anchor depths were 170 mm and 320 mm. Each combination was repeated three times to ensure repeatability.

B. DEM Model

The experimental set-up was replicated in DEM using the calibrated parameter values. The particles were allowed to settle under gravity and then levelled to the specified bed height. The anchor was then accelerated to the desired velocity over a time period of 1 second after which the velocity was kept constant. The acceleration was implemented to resemble the initial acceleration experienced during the experiments.

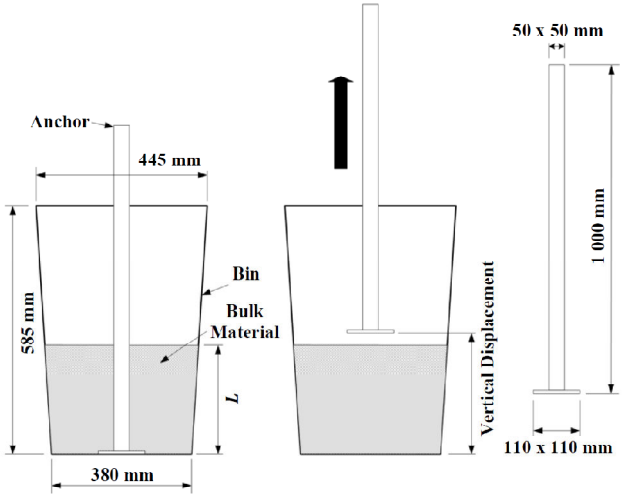

Fig. 11 The anchor pull-out test setup

C. Results

Fig. 12 shows the anchor force using a pull-out speed of 27 mm·s^{-1} and an initial anchor depth of 170 mm while Fig. 13 shows the results for an initial anchor depth of 320 mm with the same pull-out speed. Fig. 14 shows the anchor force for an initial anchor depth of 320 mm and a pull-out speed of 153 mm·s^{-1}.

The curves all show the same general trend: an initial phase where the force increased rapidly towards a peak after which it decreased towards zero as the anchor was displaced vertically and the resulting load, due to the bulk material, decreased.

In all cases the peak force obtained numerically was lower than the experimental peak force. However, the force decay curves for the experimental and numerical results corresponded well for all three cases

The smallest percentage variation in the peak anchor force was obtained for a packing height of 320 mm and anchor velocity of 27 mm·s^{-1} while the decay curve for this case also showed good results. The other combinations exhibited larger differences between the numerical and experimental results. When the higher anchor velocity was implemented in the model a larger dynamic effect was present, which could explain the larger difference between the numerical and experimental results. Also, for a lower packing depth, the numerical result showed a larger difference due to a large dynamic effect. This can be attributed to the global damping characteristics of the packing that will differ from one with a higher packing depth, due to fewer particles and therefore fewer contacts that were present. More research is needed to determine the cause of these larger discrepancies.

All the calibration tests assumed quasi-static conditions, and it was assumed to be independent of the damping ratio used. Using higher anchor velocities might induce dynamic effects not accurately modelled by the damping ratio used while with lower anchor velocities, the damping effects might not be so dominant, hence the more accurate numerical results. In future work, a method of calibrating the damping ratio should be included in the calibration procedure.

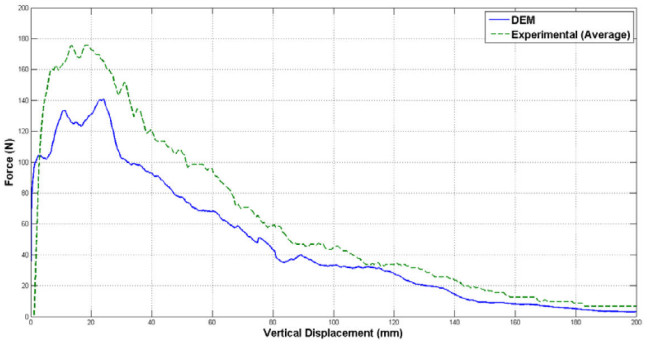

Fig. 12 The anchor pull-out force for a speed of 27 mm·s^{-1} and initial anchor depth of 170 mm

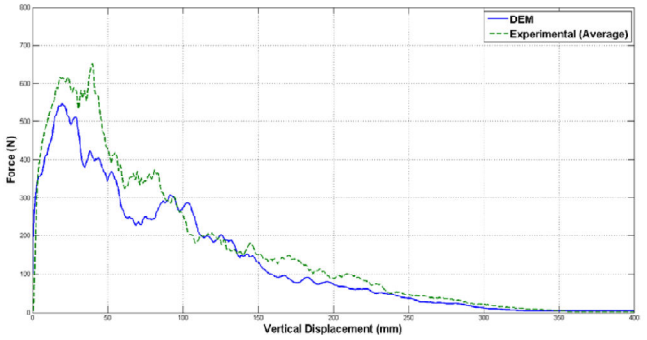

Fig. 13 The anchor pull-out force for a speed of 27 mm·s^{-1} and initial anchor depth of 320 mm

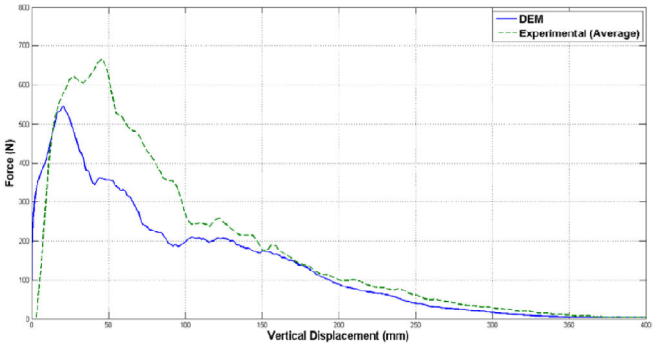

Fig. 14 The anchor pull-out force for a speed of 153 mm·s^{-1} and initial anchor depth of 320 mm

VI. Conclusion

DEM is widely used to model bulk materials handling. However, the accuracy of the models is dependent on the input parameter values. There are no standardised methods or procedures for obtaining the parameter values for a given material. The main objective of this project was to calibrate the DEM input parameters for a given coarse aggregate with particle sizes up to 40 mm as typically found in the mining and quarrying industries.

A large shear box with a diameter of 590 mm and a height of 330 mm was developed and used to perform direct shear tests on the material. The design of the shear box was such that confined compression tests could also be conducted using the same apparatus.

With the shear box as the main experimental apparatus, a calibration procedure was devised and implemented. This included the direct measurement of the particle size, particle density, the material bulk density and hence the porosity. The different particle shapes were identified through visual inspection. The shear box was used to obtain the confined Young's modulus (bulk stiffness) and the internal friction angle of the material.

DEM models, equivalent to the experimental setup, were then developed. Through an iterative procedure, the input parameter values were varied one at a time, and the bulk response recorded. The calibrated set of parameter values was defined as the set that resulted in a bulk response closest to the experimental measurements. The bulk density could be accurately modelled within 1% of the measured value, the porosity within 4%, the confined Young's modulus within 20%, and the internal friction angle within 1% of the measured values.

The combination of the test equipment developed, the calibration procedure and the DEM models developed form a useful tool for the calibration of DEM input parameter values. The benefits of efficient calibration strategies for industry and advanced academic research are significant. Using the outcomes of this project, further research and development can be done to evolve these technologies to the extent where engineers in the bulk material handling industries can use it to design, model and optimise equipment and processes.

REFERENCES

[1] L. K. Nordell, "Particle Flow Modelling: Transfer chutes and other applications," in International Materials Handling Conference (BELTCON 9), Johannesburg, South Africa, 1997.

[2] D. B. Hastie, A. P. Grima, P. W. Wypych, "Validation of particle flow through a conveyor transfer hood via particle velocity analysis," in 2nd International Conference and Exhibition on Storage, Handling and Transporting Bulk (Bulk Europe 2008), Prague, Czech Republic, 2008.

[3] T. Gröger, A. Katterfeld, "On the numerical calibration of discrete element models for the simulation of bulk solids," in Conveying and Handling of Particulate Solids (CHoPS-05), Sorrento, Italy, 2006

[4] B. Tijskens, Van Besin, Vandewalle, Ramon, "Large scale DEM," in Conveying and Handling of Particulate Solids (CHoPS-05), Sorrento, Italy, 2006.

[5] A. Grima, P. Wypych, "Investigation into calibration of discrete element model parameters for scale-up and validation of particle-structure interactions under impact conditions," Powder Technology, vol. 212, pp. 198-209, 2011.

[6] R. Annabattula, Y. Gan, M. Kamlah, "Mechanics of binary and polydisperse spherical pebble assembly," Fusion Engineering and Design, vol. 87, pp. 853-858, 2012.

[7] I. Cavarretta, C. O'Sullivan, E. Ibraim, M. Lings, S. Hamlin, D. M. Wood, "Characterization of artificial spherical particles for DEM validation studies," Particuology, vol. 10, pp. 209-220, 2012.

[8] L. Vu-Quoc, X. Zhang, O. R. Walton, "A 3-D discrete-element method for dry granular flows of ellipsoidal particles," Computational Methods in Applied Mechanics and Engineering, vol. 187, pp. 483 528, 2000.

[9] C. Gonzalez-Montellano, J. Fuentes, E. Ayuga-Tellez, F. Ayuga, "Determination of the mechanical properties of maize grains and olives required for use in DEM simulations," Journal of Food Engineering, vol. 111, pp. 553-562, 2012.

[10] C. Gonzalez-Montellano, E. Gallego, A. Rami¬rez-Gomez, F. Ayuga, "Three dimensional discrete element models for simulating the filling and emptying of silos: Analysis of numerical results," Computers & Chemical Engineering, vol. 40, pp. 22-32, 2012.

[11] C. J. Coetzee, D. N. J. Els, "Calibration of discrete element parameters and the modelling of silo discharge and bucket filling," Computers and Electronics in Agriculture, vol. 65, pp. 198-212, 2009.

[12] C. J. Coetzee, D. N. J. Els, "Calibration of granular material parameters for DEM modelling and numerical verification by blade–granular material interaction," Journal of Terramechanics, vol. 46, pp. 15–26, 2009.

[13] C. J. Coetzee, D. N. J. Els, "The numerical modelling of excavator bucket filling using DEM," Journal of Terramechanics, vol. 46, pp. 217–227, 2009.

[14] C. J. Coetzee, D. N. J. Els, G. F. Dymond, "Discrete element parameter calibration and the modelling of dragline bucket filling," Journal of Terramechanics, vol. 47, no. 1, pp. 33–44, 2010.

[15] J. Mak, Y. Chen, M. Sadek, "Determining parameters of a discrete element model for soil-tool interaction," Soil and Tillage Research, vol. 118, pp. 117-122, 2012.

[16] H. Tanaka, M. Momozu, A. Oida, M. Yamazaki, "Simulation of soil deformation and resistance at bar penetration by the distinct element method," Journal of Terramechanics, vol. 37, pp. 41-56, 2000.

[17] Y. Franco, D. Rubinstein, I. Shmulevich, "Determination of discrete element model parameters for soil-bulldozer blade interaction," in Proc. of the 15th international conference of the ISTVS, Hayama, Japan, 2005.

[18] Z. Asaf, D. Rubinstein, I. Shmulevich, "Determination of discrete element model parameters using in-situ tests and inverse solution techniques," in Proc. of the 15th international conference of the ISTVS, Hayama, Japan, September 2005.

[19] Z. Asaf, D. Rubinstein, I. Shmulevich, "Determination of discrete element model parameters required for soil tillage," Soil Till. Res., vol. 92, no. 2, pp. 227–242, 2007.

[20] Itasca, PFC3D, Particle Flow Code in 3 Dimensions, User's Guide, 4th edition, (www.itascacg.com), 2008.

[21] P. A. Cundall, O. D. L. Strack, "A discrete numerical method for granular assemblies," Geotechnique, vol. 29, pp. 47–65, 1979.

[22] O.R. Walton, R.L. Braun, "Viscosity, granular-temperature, and stress calculations for shearing assemblies of inelastic, frictional disks," J. Rheol., vol. 30, pp. 949–980, 1986.

[23] H. A. Navarro, M. P. de Souza Braun, "Determination of the normal spring stiffness coefficient in the linear spring–dashpot contact model of discrete element method," Powder Technology, vol. 246, pp. 707–722, 2013.

[24] C. J. Coetzee, S. G. Lombard, "The destemming of grapes: Experiments and discrete element modelling," Biosystems Engineering, vol. 114, pp. 232-248, 2013.

[25] P. W. Cleary, M. L. Sawley, "Three-dimensional modelling of industrial granular flows," Second International Conference on CFD in the Minerals and Process Industries, 1999.

[26] C. Hogue, "Shape representation and contact detection for discrete element simulations of arbitrary geometries," Engineering Computations, vol. 15, no. 3, pp. 374-390, 1998.

[27] D. Zhang, W. J. Whiten, "The calculation of contact forces between particles using spring and damping models," Powder Technology, vol. 88, pp. 59-64, 1996.

[28] J. W. Carson, H. Wilms, "Development of an international standard for shear testing," Powder Technology, vol. 167, no. 1, pp. 1-9, 2006.

[29] J. Härtl, J. Y. Ooi, "Experiments and simulations of direct shear tests: porosity, contact friction and bulk friction," Granular Material, vol. 10, no. 4, pp. 263-271, 2008.

[30] K. H. Head, Manual of Soil Laboratory Testing, Volume 2: Permeability, Shear Strength and Compressibility Tests, Pentech Press, London, England, 1981.

[31] J. van der Linde, Discrete element modeling of a vibratory subsoiler, M.Sc. Thesis, Department of Mechanical and Mechatronic Engineering, University of Stellenbosch, Matieland, South Africa, 2007.

[32] G. K. P. Barrios, R M. de Carvalho, A. Kwade, L. M. Tavares, "Contact parameter estimation for DEM simulation of iron ore pellet handling," Powder Technology, vol. 248, pp. 84-93, 2013.

[33] J. Wiącek, M. Molenda, J. Horabik, J. Y. Ooi, "Influence of grain shape and intergranular friction on material behavior in uniaxial compression: Experimental and DEM modeling," Powder Technology, vol. 217, pp. 435–442, 2012.

[34] A. Grima, P. Wypych, "Development and validation of calibration methods for discrete element modelling," Granular Matter vol. 13, pp. 127-132, 2011b.

[35] M. Obermayr, C. Vrettos, P. Eberhard, T. Dauwel, "A discrete element model and its experimental validation for the prediction of draft forces in cohesive soil," Journal of Terramechanics, vol. 53, pp.93–104, 2014.
[36] M. Ucgul, J. M. Fielke, C. Saunders, "Three-dimensional discrete element modelling of tillage: Determination of a suitable contact model and parameters for a cohesionless soil," Biosystems Engineering, vol. 121, pp. 105-117, 2014.
[37] K. H. Head, Soil Technicians' Handbook, London, Pentech Press, 1989.
[38] C. J. Coetzee, R. G. Nel, "Calibration of discrete element properties and the modelling of packed rock beds," Powder Technology, vol. 264, pp. 332–342, 2014.
[39] A. F. Cabalar, "Applications of the oedometer, triaxial and resonant column tests to the study of micaceous sands," Engineering Geology, vol. 112, pp. 21–28, 2010.
[40] Y-C. Chung, J. Y. Ooi, "A study of influence of gravity on bulk behaviour of particulate solid," Particuology, vol. 6, pp. 467–474, 2008.
[41] Y. Xu, K. D. Kafui, C. Thornton, G. Lian, "Effects of Material Properties on Granular Flow in a Silo Using DEM Simulation," Particulate Science and Technology, vol. 20 pp. 109-124, 2002.
[42] S. Lommen, D. Schott, G. Lodewijks, "DEM speedup: Stiffness effects on behavior of bulk material," Particuology, vol. 12, pp. 107-112, 2014.
[43] J. Härtl, J. Y. Ooi, "Experiments and simulations of direct shear tests: porosity, contact friction and bulk friction," Granular Matter, vol. 10, pp. 263–271, 2008.